Mice harboring the human *SLC30A8* R138X loss-of-function mutation have increased insulin secretory capacity

Sandra Kleiner[a], Daniel Gomez[a], Bezawit Megra[a], Erqian Na[a], Ramandeep Bhavsar[a], Katie Cavino[a], Yurong Xin[a], Jose Rojas[a], Giselle Dominguez-Gutierrez[a], Brian Zambrowicz[a], Gaelle Carrat[b], Pauline Chabosseau[b], Ming Hu[b], Andrew J. Murphy[a], George D. Yancopoulos[a,1], Guy A. Rutter[b], and Jesper Gromada[a,1]

[a]Regeneron Pharmaceuticals, Inc., Tarrytown, NY 10591; and [b]Section of Cell Biology and Functional Genomics, Division of Diabetes, Endocrinology and Metabolism, Imperial Centre for Translational and Experimental Medicine, Imperial College London, London W12 0NN, United Kingdom

Contributed by George D. Yancopoulos, May 23, 2018 (sent for review December 11, 2017; reviewed by Philipp E. Scherer and Gordon C. Weir)

***SLC30A8* encodes a zinc transporter that is primarily expressed in the pancreatic islets of Langerhans. In β-cells it transports zinc into insulin-containing secretory granules. Loss-of-function (LOF) mutations in *SLC30A8* protect against type 2 diabetes in humans. In this study, we generated a knockin mouse model carrying one of the most common human LOF mutations for *SLC30A8*, R138X. The R138X mice had normal body weight, glucose tolerance, and pancreatic β-cell mass. Interestingly, in hyperglycemic conditions induced by the insulin receptor antagonist S961, the R138X mice showed a 50% increase in insulin secretion. This effect was not associated with enhanced β-cell proliferation or mass. Our data suggest that the *SLC30A8* R138X LOF mutation may exert beneficial effects on glucose metabolism by increasing the capacity of β-cells to secrete insulin under hyperglycemic conditions.**

SLC30A8 | genetic mutation | insulin secretion | pancreatic beta cell | zinc transporter

SLC30A8 is a zinc transporter (ZnT8) located in the islet cells of the endocrine pancreas. In β-cells, SLC30A8 transports zinc into the insulin-containing granules. Two zinc ions bind with and stabilize a hexameric form of insulin, triggering insulin crystallization (1). While loss of SLC30A8 substantially decreases islet zinc content and insulin crystallization (2, 3), its effects on secretion and regulation of glucose metabolism are still unclear. Several groups have generated *Slc30a8* knockout (KO) mouse models either globally or restricted to pancreatic β-cells. The observed metabolic phenotype of some, but not all, of these models shows mild impairment of glucose tolerance associated with reduced or unchanged plasma insulin levels (4). Importantly, none of these earlier studies reported beneficial effects associated with *Slc30a8* deficiency. Therefore, it came as a surprise when Flannick and colleagues (5) reported that haploinsufficiency of *SLC30A8* is protective against the development of type 2 diabetes (T2D) in humans. Their study identified 12 putative loss-of-function (LOF) variants that collectively decreased the risk for T2D by 65%. One of the most abundant variants, p. Arg138* (from here on called R138X), causing a premature stop codon, was individually associated with protection from T2D and reported to encode an unstable protein (5). Thus, mouse and human data seemingly contradict each other, and it is unclear how the rare LOF variants reduce the risk of T2D. To investigate this, we generated an *Slc30a8* mouse model carrying the R138X mutation as a representative human LOF variant. Interestingly, we found that the β-cells in the R138X mice have an extraordinary capacity to secrete insulin in response to severe hyperglycemia.

Results

R138X Islets Show Loss of Slc30a8 Function Despite Partial Protection of the R138X Transcript. To investigate how *SLC30A8* LOF variants influence the risk of T2D, we altered codon 137 (equivalent to codon 138 in humans) of *Slc30a8* in the mouse genome from CGA to TGA, exchanging the arginine for a stop codon (*R138X*). The R138X mice were born at the expected Mendelian ratio without obvious growth abnormalities. RNA in situ hybridization showed strong *Slc30a8* mRNA staining in pancreatic islets from wild-type (WT) mice but no staining in islets from homozygous *Slc30a8* KO mice, validating the specificity of the probe (Fig. 1*A*). In contrast to islets from *Slc30a8* KO mice, islets from R138X mice showed a substantial amount of *Slc30a8* RNA staining (Fig. 1*A*). Quantification of *Slc30a8* mRNA using real-time PCR revealed a 70% reduction in R138X islets, although the absolute *Slc30a8* transcript level in the R138X islets [cycle threshold (CT) value 22.2] was still high and comparable to the expression level of the housekeeping gene *Gapdh* (CT value 22.1) (Fig. 1*B*). The presence of this high level of *Slc30a8* RNA in the R138X mice suggests that the R138X transcript cannot effectively be degraded by nonsense-mediated mRNA decay, a process that degrades mRNAs carrying a premature translation termination codon (6).

Significance

The zinc transporter SLC30A8 is primarily expressed in islets of the endocrine pancreas. Human *SLC30A8* loss-of-function mutations protect against type 2 diabetes. However, *Slc30a8* knockout mice do not show this protection. We have generated a mouse model mimicking a common protective human *SLC30A8* loss-of-function allele. This mouse model shows a beneficial effect of loss of SLC30A8 function on β-cell biology. In particular, mice carrying the protective R138X allele have an increased capacity to secrete insulin in high-glucose conditions. Understanding the signaling mechanisms regulating insulin secretion in the R138X mice could provide novel insights into β-cell biology, and may lead to the identification of therapeutic targets for the treatment of diabetes.

Author contributions: S.K. and J.G. designed research; D.G., B.M., E.N., R.B., K.C., and J.R. performed research; S.K., D.G., B.M., E.N., R.B., Y.X., G.D.-G., and J.G. analyzed data; and S.K., B.Z., G.C., P.C., M.H., A.J.M., G.D.Y., G.A.R., and J.G. wrote the paper.

Reviewers: P.E.S., University of Texas Southwestern Medical Center; and G.C.W., Joslin Diabetes Center, Harvard Medical School.

Conflict of interest statement: S.K., D.G., B.M., E.N., R.B., K.C., Y.X., J.R., G.D.-G., B.Z., A.J.M., G.D.Y., and J.G. are employees and shareholders of Regeneron Pharmaceuticals, Inc.

Data deposition: The data reported in this paper have been deposited in the Gene Expression Omnibus (GEO) database, https://www.ncbi.nlm.nih.gov/geo (accession no. GSE114207).

[1]To whom correspondence may be addressed. Email: george@regeneron.com or jesper.gromada@regeneron.com.

This article contains supporting information online at www.pnas.org/lookup/suppl/doi:10.1073/pnas.1721418115/-/DCSupplemental.

Published online July 23, 2018.

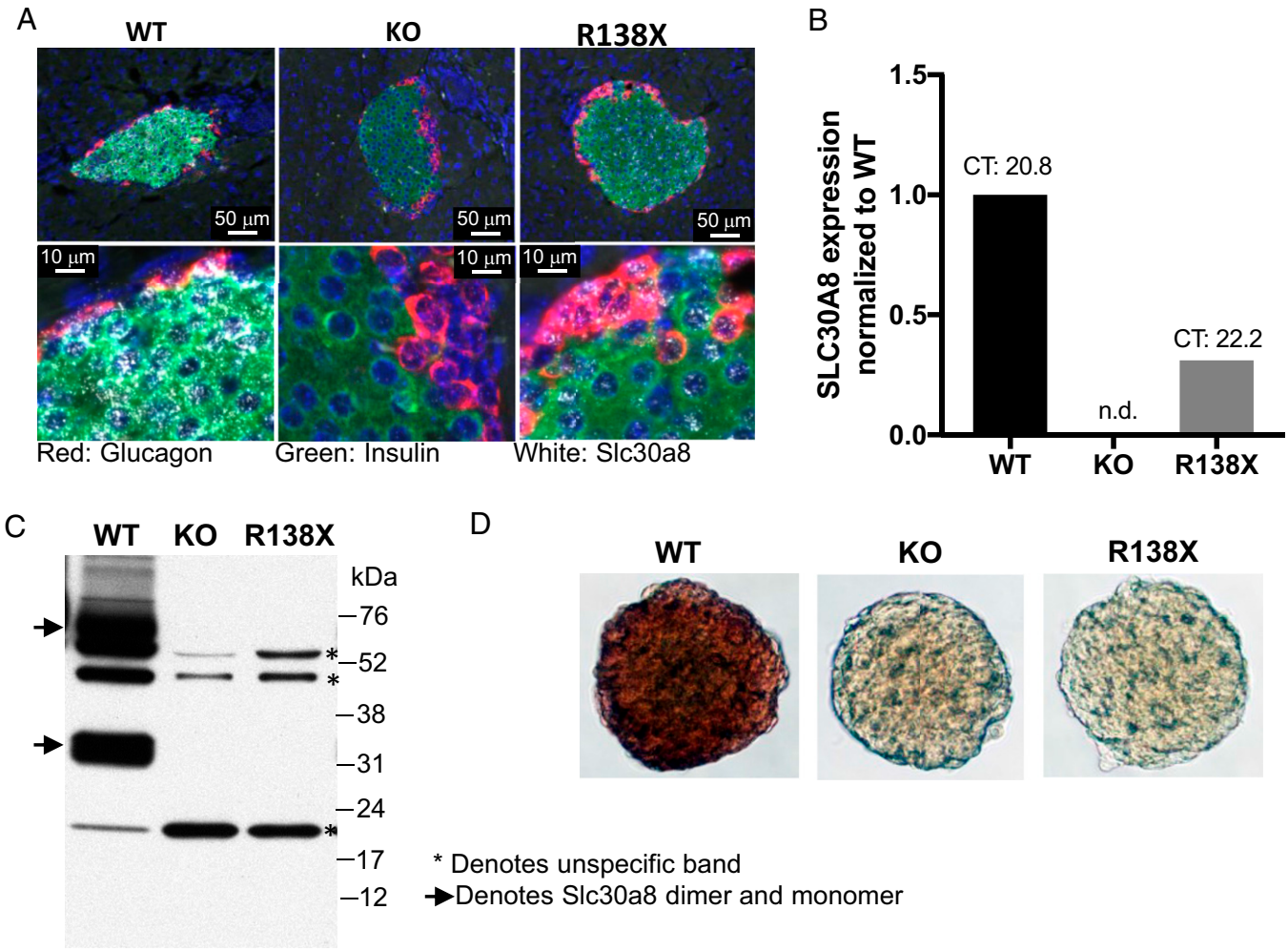

Fig. 1. Analysis of *Slc30a8* RNA and protein in islets from male R138X mice on chow diet. (*A*) *Slc30a8* RNA in situ hybridization of pancreatic islets isolated from wild-type, knockout, and R138X mice. KO islets were used as negative control. Red, glucagon RNA; green, insulin RNA; white, *Slc30a8* RNA. (*B*) Quantification of islet *Slc30a8* RNA levels using qPCR analysis. n.d., not detected. (*C*) Western blot of islets isolated from chow-fed WT, KO, and R138X mice. KO islets were used as negative control. The arrow indicates SLC30A8 protein; asterisks denote unspecific bands. (*D*) Dithizone staining of pancreatic islets isolated from WT, KO, and R138X mice.

To determine whether the detected RNA in the R138X mice is translated into a truncated protein, we performed Western (immuno)blotting for SLC30A8 protein using an antibody raised against an N-terminal peptide of the mouse protein. We were not able to identify a truncated protein at the expected molecular mass (~16 kDa for the monomer) in lysates from isolated islets (Fig. 1*C*), despite being able to detect the R138X protein and stabilize it by proteasomal inhibition when overexpressed in HEK293 cells (*SI Appendix*, Fig. S1). In addition, zinc staining using dithizone revealed that islets from R138X and KO mice were zinc-depleted, demonstrating the absence of a functional SLC30A8 protein in both mouse lines (Fig. 1*D*). In summary, introduction of the human R138X LOF variant into the mouse *Slc30a8* gene results in loss of function.

R138X Mice on Chow Diet Have a Normal Metabolic Phenotype. We first investigated whether the introduction of the R138X stop codon altered metabolic parameters in chow-fed mice. WT and R138X mice did not differ in their body weight or circulating blood glucose or insulin levels (Fig. 2 *A*–*C*). In addition, circulating proinsulin and C-peptide levels were similar between WT and R138X mice (*SI Appendix*, Fig. S2 *A* and *B*). While the ratio of proinsulin to C peptide did not change, we did observe a mild decrease in the ratio of insulin to C peptide, suggesting higher insulin clearance in R138X mice similar to what has been observed in *Slc30a8* KO mice (*SI Appendix*, Fig. S2*D*) (7). Glucose tolerance and insulin sensitivity were similar in the R138X and control mice, and we did not observe changes in glucose-induced insulin secretion (Fig. 2 *D*–*F*). In addition, the absence of islet zinc did not affect islet morphology, as β-cell and α-cell masses were not altered (Fig. 2 *G* and *H* and *SI Appendix*, Fig. S2 *E* and *F*). Taken together, these data show that the R138X LOF variant does not affect glucose homeostasis or glucose-induced insulin secretion in chow-fed mice.

R138X Mice Have Increased Insulin Secretion in Response to Insulin Receptor Inhibition-Induced Hyperglycemia. Next, we wanted to investigate a potential effect of the R138X mutation in metabolically challenged mice. We used the insulin receptor antagonist S961 to induce severe insulin resistance and hyperglycemia (8). As expected, S961 caused hyperglycemia (~600 mg/dL) in all treated animals, while the control animals kept normal-fed glucose levels (~200 mg/dL) (Fig. 3*A*). Circulating insulin levels rose in response to S961 in all treated mice. Strikingly, R138X mice had more than 50% (WT: 42.33 ± 5.03 ng/mL; R138X: 67.75 ± 19.16 ng/mL) higher plasma insulin levels upon S961-induced

PHYSIOLOGY

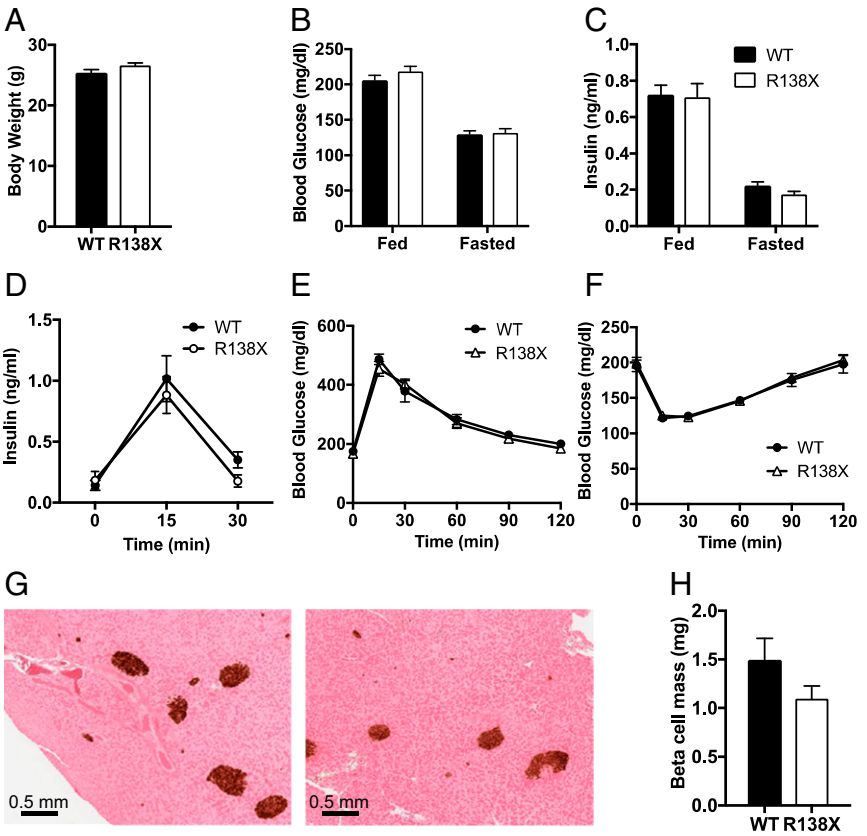

Fig. 2. Metabolic phenotype of male R138X mice on chow diet. (*A–C*) Body weight (*A*), blood glucose (*B*), and plasma insulin (*C*) in fed and fasted WT and R138X mice ($n = 18$ to 20 per genotype). (*D*) Plasma insulin levels in WT or R138X mice after an overnight fast (time 0) and at the indicated times after an i.p. injection of glucose. Data are displayed as blood insulin levels over time ($n = 6$ per genotype). (*E*) Oral glucose tolerance test in overnight-fasted (time 0) WT and R138X mice. Data are displayed as blood glucose over time ($n = 6$ per genotype). (*F*) Insulin tolerance test in 4-h-fasted WT and R138X mice. Data are displayed as blood glucose levels over time ($n = 6$ per genotype). (*G*) Histology for insulin in pancreas isolated from WT and R138X mice. (*H*) Quantification of pancreatic insulin staining ($n = 6$ per genotype). Values represent the means ± SEM. Data were analyzed by two-way ANOVA or Student's *t* test. No significance was reached.

hyperglycemia compared with S961-treated WT mice (Fig. 3*B*). The increase in plasma insulin was not a result of improved proinsulin processing or decreased insulin clearance (*SI Appendix*, Fig. S3 *A–E*) or changes in circulating GLP-1 levels between R138X and WT mice (Fig. 3*C*). Circulating insulin was higher in fed and fasted conditions in R138X mice treated with S961 but blood glucose levels did not differ between genotypes, because of the inhibition of insulin action on the insulin receptor by S961 (Fig. 3 *D* and *E*). Of note, fasted insulin levels were substantially elevated with S961 treatment in WT and R138X mice compared with PBS-treated mice, despite normal fasting blood glucose levels.

To investigate whether the higher insulin levels in the mutant mice were a consequence of increased β-cell proliferation, we measured Ki-67 staining in insulin-positive β-cells. While β-cell proliferation clearly increased with S961 treatment, there was no difference in β-cell proliferation between R138X and WT mice (Fig. 3 *F* and *G*). Consistent with the proliferation data, there was no difference in β- or α-cell mass in S961-treated WT and R138X mice (Fig. 3 *F* and *H* and *SI Appendix*, Fig. S3 *F* and *G*). Despite the large increase in blood insulin, β-cells from S961-treated R138X mice did not appear to be more insulin-depleted than β-cells from S961-treated WT mice (Fig. 3*F*). In summary, these data suggest that islets from the R138X mice have a higher capacity to secrete insulin when challenged with hyperglycemia.

Islets from R138X Mice Have Decreased Mitochondrial Gene Expression and Increased *Hvcn1* Expression. To understand the differences between WT and R138X islets in more detail, we performed RNA sequencing (RNA-seq) on islets isolated from chow-fed mice. In confirmation with our RNAscope and TaqMan data (Fig. 1 *A* and *B*), the amount of *Slc30a8* mRNA was strongly reduced [from ∼500 reads per kilobase of transcript per million mapped reads (RPKM) in WT to ∼100 RPKM in R138X] but not absent (*SI Appendix*, Fig. S4). Using a minimum read count of 10 for each sample of the higher-expressing group as a cutoff, we found a total of 12,831 genes expressed in the isolated islets. Out of these 12,831 genes, only 61 genes (18 genes increased, 43 genes decreased) were differentially regulated using a cutoff of 1.5-fold expression difference and a P value <0.01 in R138X islets (Table 1). Interestingly, this list does not contain genes involved in zinc metabolism or insulin biosynthesis. However, the expression of insulin 2 (*Ins2*) was significantly down-regulated and the expression of insulin 1 (*Ins1*) trended lower, too (Fig. 4*A*). This prompted us to look more carefully into the expression of β-cell regulators, including transcription factors for insulin. As shown in Fig. 4*B*, *Mafa* was significantly up-regulated in islets of R138X mice but missed our cutoff of 1.5-fold. Since *Mafa* positively regulates insulin transcription and its expression is usually positively associated with the expression of the hormone (9), it does not explain the reduced *Ins2* gene expression but rather compensation to the low *Ins2* expression. Out of the 43 down-regulated genes, 12 genes were mitochondrial proteins and 7 belonged to the group of Oxphos genes (Table 1). We therefore analyzed all Oxphos genes and noted that the expression of most of these genes was reduced (Table 2 and *SI Appendix*, Table S1). Complexes I, III,

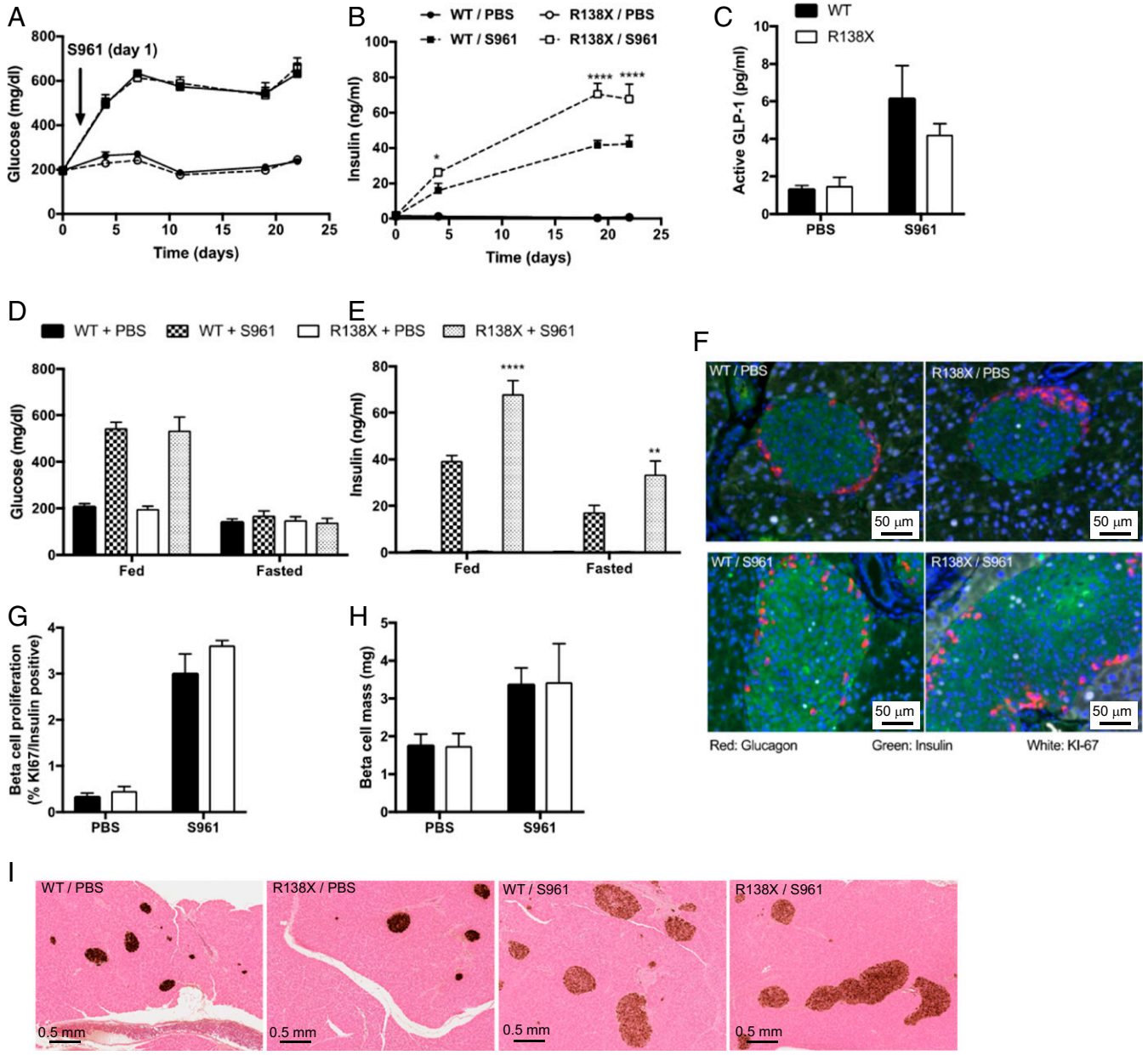

Fig. 3. R138X mice secrete more insulin under chronic hyperglycemia caused by the insulin receptor antagonist S961. (*A*) Nonfasted plasma glucose levels in R138X and WT mice continuously treated with the insulin receptor antagonist S961 (20 nmol/wk) or PBS for 22 d. (*B*) Nonfasted plasma insulin on day 0, 4, 19, and 22 R138X and WT mice treated with S961 (20 nmol/wk) or PBS. (*C*) Plasma active GLP-1 levels in WT and R138X mice after 22 d of treatment. (*D* and *E*) Fed and fasted glucose (*D*) and insulin (*E*) levels measured day 19 and 20 after initiation of treatment. (*F*) Immunohistochemistry for Ki-67 (white), insulin (green), and glucagon (red). (*G*) Quantification of Ki-67 and insulin double-positive cells. (*H*) Quantification of pancreatic insulin staining shown in *I*. (*I*) Histology for insulin in pancreas isolated from WT and R138X mice after 22 d of treatment. Values represent the means ± SEM ($n = 5$ to 7 mice per treatment and genotype). $^{*}P < 0.5$, $^{**}P < 0.01$, $^{****}P < 0.0001$.

and V were mainly affected with a reduction in gene expression of about 40%, suggesting a reduced capacity to generate ATP.

Of note, the expression of the voltage-gated proton channel Hv1 (Hvcn1; alternate names VSOP, HV1) was up-regulated in islets from R138X mice. Since this channel is Zn^{2+}-regulated and present in the insulin secretory granules and loss of *Hvcn1* expression impairs insulin secretion in vivo and in vitro (10–12), this channel might be important for the observed phenotype in the R138X mice.

Discussion

In this study, we generated an *Slc30a8* LOF mouse model (R138X mice) mimicking one of the two most common human *SLC30A8* LOFs (p.Arg138*) (5). Using this model, we show that the introduction of the R138X mutation results in the secretion of 50% more insulin in response to hyperglycemia. These data suggest that SLC30A8 LOF can have beneficial effects on pancreatic β-cells by increasing the insulin secretory capacity and allowing the β-cells to better compensate for enhanced insulin demand. The present approach emphasizes the utility of mouse genetics to explore the mechanisms of genetic variants which affect the risk of T2D in humans.

More than eight different *Slc30a8* KO mouse models have been reported (2, 3, 7, 13–16). These models vary in genetic background, *Slc30a8* targeting strategy, and the specific Cre line that was used when mice with β-cell–specific deletions were generated. The metabolic phenotypes of these mice vary too.

Table 1. Differentially regulated genes in islets from chow-fed WT and R138X mice

Gene ID	Symbol	Fold change	*P* value	Description
170942	*Erdr1*	3.34	9.80E-04	Erythroid differentiation regulator 1
74096	*Hvcn1*	2.87	3.90E-03	Hydrogen voltage-gated channel 1
12483	*Cd22*	2.79	2.70E-03	CD22 antigen
19354	*Rac2*	2.63	6.60E-04	RAS-related C3 botulinum substrate 2
12265	*Ciita*	2.47	2.50E-03	Class II transactivator
17691	*Sik1*	2.37	7.10E-08	Salt-inducible kinase 1
18636	*Cfp*	2.01	7.50E-03	Complement factor properdin
17318	*Mid1*	1.79	1.70E-03	Midline 1
170935	*Grid2ip*	1.75	8.60E-03	Glutamate receptor, ionotropic, delta 2 (Grid2) interacting protein 1
666048	*Trabd2b*	1.72	4.20E-03	TraB domain-containing 2B
11899	*Astn1*	1.67	1.60E-03	Astrotactin 1
23984	*Pde10a*	1.66	4.50E-03	Phosphodiesterase 10A
244723	*Olfm2*	1.62	7.40E-03	Olfactomedin 2
17294	*Mest*	1.60	8.30E-04	Mesoderm specific transcript
319504	*Nrcam*	1.56	6.10E-06	Neuron-glia-CAM-related cell adhesion molecule
104601	*Mycbpap*	1.53	3.80E-03	MYCBP associated protein
12545	*Cdc7*	1.53	8.00E-03	Cell division cycle 7 (*Saccharomyces cerevisiae*)
544817	*Arhgap27*	1.52	3.50E-03	Rho GTPase activating protein 27
319760	*D130020L05Rik*	−1.52	1.10E-03	RIKEN cDNA D130020L05 gene
195531	*Gm13152*	−1.54	3.40E-03	Predicted gene 13152
66091	***Ndufa3***	**−1.54**	**1.20E-03**	**NADH dehydrogenase (ubiquinone) 1 alpha subcomplex, 3**
16334	*Ins2*	−1.54	7.20E-03	Insulin II
235043	*Tmem205*	−1.54	8.70E-03	Transmembrane protein 205
14470	*Rabac1*	−1.56	2.90E-03	Rab acceptor 1 (prenylated)
14776	*Gpx2*	−1.59	1.80E-07	Glutathione peroxidase 2
66416	***Ndufa7***	**−1.59**	**6.20E-03**	**NADH dehydrogenase (ubiquinone) 1 alpha subcomplex, 7 (B14.5a)**
228715	*Gm561*	−1.59	6.90E-03	Predicted gene 561
66845	***Mrpl33***	**−1.59**	**2.10E-03**	**Mitochondrial ribosomal protein L33**
17178	*Fxyd3*	−1.59	3.10E-03	FXYD domain-containing ion transport regulator 3
20832	*Ssr4*	−1.59	6.40E-03	Signal sequence receptor, delta
66594	***Uqcr11***	**−1.61**	**7.50E-03**	**Ubiquinol-cytochrome *c* reductase, complex III subunit XI**
66152	***Uqcr10***	**−1.61**	**7.30E-03**	**Ubiquinol-cytochrome *c* reductase, complex III subunit X**
67267	***Uqcc2***	**−1.61**	**7.60E-03**	**Ubiquinol-cytochrome *c* reductase complex assembly factor 2**
69038	*Tmem258*	−1.61	4.60E-03	Transmembrane protein 258
67885	*1500011K16Rik*	−1.61	9.30E-03	RIKEN cDNA 1500011K16 gene
100502825	*Rpl37rt*	−1.61	5.40E-03	Predicted gene 13826
66117	*1110001J03Rik*	−1.61	4.40E-03	RIKEN cDNA 1110001J03 gene
69094	*Tmem160*	−1.61	8.50E-03	Transmembrane protein 160
67941	*Rps27l*	−1.61	4.00E-03	Ribosomal protein S27-like
234421	*Cib3*	−1.64	5.30E-03	Calcium and integrin binding family member 3
11807	*Apoa2*	−1.67	3.80E-04	Apolipoprotein A-II
20892	*Stra13*	−1.67	2.90E-03	Stimulated by retinoic acid 13
66477	***Usmg5***	**−1.67**	**5.60E-03**	**Up-regulated during skeletal muscle growth 5**
68563	***Dpm3***	**−1.67**	**2.50E-03**	**Dolichyl-phosphate mannosyltransferase polypeptide 3**
22177	*Tyrobp*	−1.67	9.90E-03	TYRO protein tyrosine kinase binding protein
69386	*Hist1h4h*	−1.69	5.00E-03	Histone cluster 1, H4h
268686	*S100z*	−1.69	9.90E-04	S100 calcium binding protein, zeta
73720	*Cst6*	−1.69	2.80E-03	Cystatin E/M
27425	***Atp5l***	**−1.69**	**4.90E-03**	**ATP synthase, H^+ transporting, mitochondrial F0 complex, subunit G**
68194	***Ndufb4***	**−1.72**	**4.70E-03**	**NADH dehydrogenase (ubiquinone) 1 beta subcomplex 4**
449000	*Zfp960*	−1.72	1.30E-03	Zinc finger protein 960
93757	***Immp2l***	**−1.75**	**3.20E-03**	**IMP2 inner mitochondrial membrane peptidase-like (*S. cerevisiae*)**
19735	*Rgs2*	−1.82	7.40E-03	Regulator of G protein signaling 2
17873	*Gadd45b*	−1.82	1.40E-04	Growth arrest and DNA-damage-inducible 45 beta
20335	*Sec61g*	−1.82	3.20E-03	SEC61, gamma subunit
13190	*Dct*	−1.89	4.10E-04	Dopachrome tautomerase
11811	*Apobec2*	−1.89	3.30E-03	Apolipoprotein B mRNA editing enzyme, catalytic polypeptide 2
100169864	*SlcUbl4a*	−2.13	2.90E-05	Slc10a3-Ubl4 read-through
19782	***Rmrp***	**−2.17**	**8.40E-03**	**RNA component of mitochondrial RNase P**
100568459	*Bc1*	−2.27	4.10E-03	Brain cytoplasmic RNA 1
239436	*Slc30a8*	−6.67	1.40E-43	Solute carrier family 30 (zinc transporter), member 8

Mitochondrial genes are marked in bold.

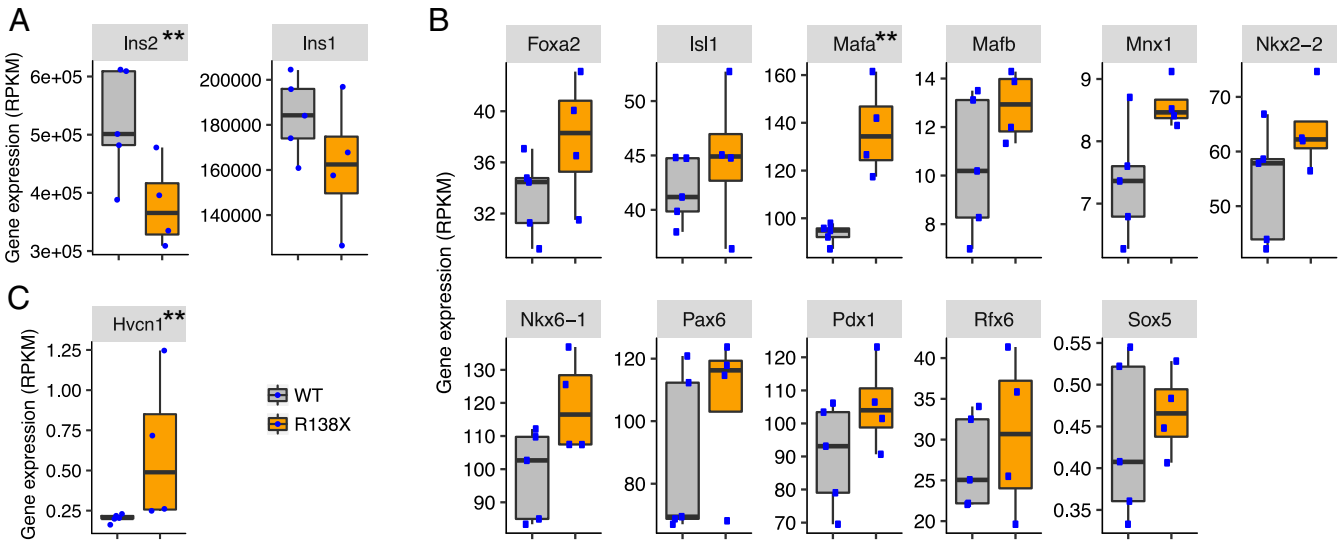

Fig. 4. Gene expression in islets from WT versus R138X mice. (*A*) RPKM values for insulin 2 and insulin 1. (*B*) RPKM values for β-cell regulators. (*C*) RPKM values for *Hvcn1*. $^{**}P < 0.01$ defined by DESeq2 (Wald test) (24).

Differences in body weight gain, glucose tolerance, and insulin secretion have been reported on chow and high-fat diets (4). However, all *Slc30a8* KO phenotypes show either no change or a decrease in circulating insulin, which was in some instances associated with worsening of glucose tolerance (3, 13, 17). On the contrary, an increase in in vitro insulin secretion has been observed in islets from three KO models (3, 7, 16). We did not observe a major metabolic phenotype, including a change in glucose-induced insulin secretion in chow-fed R138X mice. When challenged with S961, however, these mice were able to secrete much more insulin than their WT counterparts. This increase in insulin secretion was not secondary to an increase in β-cell mass and has not been reported in any of the *Slc30a8* KO models. Currently, it is unclear whether the R138X mice are like *Slc30a8* KO mice, since we cannot rule out that the remaining mRNA is translated into a truncated protein. We have not been able to detect a truncated protein in the islets of the R138X mice. However, the RNA is present, and overexpressed R138X protein was detected in HEK293 cells and accumulated after proteasomal inhibition (*SI Appendix*, Fig. S1). Thus, we cannot exclude the existence of low levels of protein, perhaps in a subset of the islet cells from the R138X mice. Independent of the potential expression of small amounts of truncated R138X protein, dithizone staining showed that the R138X LOF mutation resulted in loss of islet zinc consistent with observations in *Slc30a8* KO mice.

How is insulin secretion up-regulated in R138X mice? The easiest explanation is through up-regulation of the voltage-gated proton channel Hvcn1. Hvcn1 is present in secretory granules and inhibited by zinc ions (12). In addition, *Hvcn1* KO mice have decreased insulin secretion and impaired glucose homeostasis (11). Since islets from the R138X mice are zinc-depleted, one would expect an increase in the activity of this channel. On top of that, we see a threefold up-regulation of the *Hvcn1* transcript in islets from R138X mice. While these data suggest that the increase in insulin secretion is at least in part mediated by Hvcn1, further experiments have to validate this hypothesis. Another interesting finding is the reduction of mitochondrial gene expression in R138X mice. This seems counterintuitive, since ATP synthesis is required for proper insulin secretion (18). However, a recent paper described a novel pathway to activate insulin secretion in β-cells (19). This pathway is independent of ATP synthesis (oligomycin-resistant) but depends on permissive cytosolic Ca^{2+} concentration. It is accompanied by a small reduction in mitochondrial glutathione and is mediated by activating mitochondrial complex II. This is interesting, taking into consideration that *Gpx2* (glutathione peroxidase 2) expression (Table 1) and only one gene from Oxphos complex II had reduced expression in the R138X mice. This pathway, in addition to the established "amplifying" pathway for glucose-induced insulin secretion (20), as well as a pathway dependent upon cytosolic NAD(P)H generation (21), may thus contribute to the enhanced insulin secretory actions of the R138X variant. Of note, deletion of liver kinase B1 (LKB1) selectively in β-cells (22) leads to marked mitochondrial defects and impaired Ca^{2+} dynamics, while glucose-stimulated insulin secretion is enhanced, most likely due to the up-regulation of the novel ATP synthesis-independent pathways described above. Again, further experiments examining respiration and insulin secretion are required to investigate whether this alternative pathway is predominately used in β-cells from R138X mice.

In conclusion, our data from the R138X mice show that loss of SLC30A8 function can exert beneficial effects on β-cells consistent with the protective effect of SLC30A8 LOF mutations in humans (5). It therefore seems to be a relevant model to study the mechanism underlying this protection. While it is tempting to speculate that the enhanced capacity to secrete insulin explains some of the observed protection seen in humans, further experiments in mice in settings mimicking T2D will have to be performed to validate this claim. In addition, experiments on heterozygous mice are required to prove that the enhanced insulin secretory capacity is present with haploinsufficiency as seen in humans.

Methods

Animals. All procedures were conducted in compliance with protocols approved by the Regeneron Pharmaceuticals Institutional Animal Care and Use Committee. The *Slc30a8* R138X and knockout mouse lines were made in a

Table 2. Summary of Oxphos gene expression changes in islets of WT and R138X mice

Complex	Total	Significantly regulated ($P < 0.05$)	Regulated, %
I	43	19	44
II	4	1	25
III	10	4	40
IV	19	5	26
V	20	9	45

PHYSIOLOGY

100% C57BL/6NTac background using VelociGene technology (23). For the generation of the knockout mouse line, the whole *Slc30a8*-coding region was deleted and replaced with a *LacZ* gene. The neomycin gene was removed through the use of a self-deleting neomycin selection cassette. For the generation of the R138X mice, nucleotide 409 was changed from C to T in exon 3, which changes the arginine into a stop codon. The mutated allele has a self-deleting neomycin selection cassette flanked by loxP sites inserted at intron 3, deleting 29 bp of endogenous intron 3 sequence. Mice were housed (up to five mice per cage) in a controlled environment (12-h light/dark cycle, 22 ± 1 °C, 60 to 70% humidity) and fed ad libitum with chow (Purina Laboratory 23 Rodent Diet 5001; LabDiet). All data shown are compared with WT littermates.

Glucose and Insulin Tolerance Tests. For oral glucose tolerance tests (oGTT), mice were fasted overnight (16 h) followed by oral gavage of glucose (Sigma) at 2 g/kg body weight. For insulin tolerance tests, mice were fasted in the morning for 4 h followed by i.p. injection of 0.75 U/kg of human insulin (Eli Lilly). Blood samples for glucose measurements were obtained from the tail vein at the indicated times, and glucose levels were measured using the AlphaTRAK 2 glucometer (Abbott). For insulin measurements, submandibular bleeds were done at 0, 15, and 30 min postinjection in separate experiments to not interfere with glucose measurements.

Plasma Insulin, Proinsulin, and C-Peptide Measurements. Submandibular bleeds of either overnight-fasted or fed animals were done in the morning or following an oGTT. Insulin was analyzed with mouse insulin ELISA (Mercodia). Proinsulin was analyzed with mouse proinsulin ELISA (Mercodia). C peptide was analyzed with mouse C-peptide ELISA (ALPCO). All ELISAs were performed according to the manufacturer's instructions.

Histology. Pancreata were fixed in 10% neutral buffered formalin solution for 48 h and then embedded in paraffin. Two sections of the pancreas from each animal were stained with an α-glucagon (REGN745; a monoclonal antibody generated in-house) or an α-insulin (Dako) antibody, and areas of glucagon- and insulin-positive cells were measured using HALO digital imaging analysis software (Indica Labs). The percentages of glucagon- and insulin-positive areas in proportion to the whole pancreas area were calculated. Taking the area as basis, α-cell mass was calculated by multiplying the α-cell area for each animal by the weight of the animal's pancreas. To quantify β-cell area, islet number and size were measured by counting the number of insulin-positive islets in a section. The analysis was set to capture every cluster of insulin-positive cells down to a single-cell resolution. Every stained area larger than 150 μm^2 was counted as an islet. We excluded artifacts (e.g., debris) smaller than one single β-cell (<150 μm^2; area was calculated using a diameter of about 14 μm). The total β-cell area was calculated by multiplying the average islet size by the number of islets (normalized to pancreas area). This value was then multiplied by the individual pancreas weight to get the β-cell mass. For fluorescence staining, pancreas sections were stained with a combination of α-insulin antibody (A0564; Dako) and α–Ki-67 antibody (R&D) followed by appropriate secondary antibodies. Fluorescent signal was detected using a microscope slide scanner (Zeiss Axio Scan.Z1). Islet cell types were quantified using HALO image analysis using the CytoNuclear Fluorescence module (Indica Labs). Insulin and Ki-67 double-positive cells were counted and expressed as the percent of insulin-positive cells.

RNA in Situ Hybridization. For RNA analysis, pancreas tissue was permeabilized and hybridized with combinations of mRNA probes for mouse *Gcg*, *Ins2*, and *Slc30a8* according to the manufacturer's instructions (Advanced Cell Diagnostics). A fluorescence kit was used to amplify the mRNA signal. Fluorescent signal was detected using a microscope slide scanner (Zeiss Axio Scan.Z1).

Islet Isolation and Dithizone Staining. Mouse islets were isolated by density gradient separation after perfusing the pancreas with Liberase TL (05401020001; Roche) through the common bile duct. Following a 13-min digestion at 37 °C, the pancreas solution was washed and filtered through a 400-μm wire mesh strainer and islets were separated by Histopaque gradient centrifugation at 1217 × *g* (H 1077; Sigma-Aldrich). Isolated islets were cultured overnight in RPMI-1640 medium (Gibco) supplemented with 10% (vol/vol) FBS, 10 mM Hepes, 50 μM β-mercaptoethanol, 1.0 mM sodium pyruvate, 100 U/mL penicillin, and 100 μg/mL streptomycin at 37 °C with a 5% CO_2 in air atmosphere. Up to 50 islets were hand-picked and transferred to a new dish containing 100 μg/mL dithizone solution. Islets were stained for up to 10 min and transferred back into a PBS solution for microscopy (Zeiss confocal microscope).

Western (Immuno)Blot Analysis. Islets were lysed in RIPA lysis buffer and the protein concentration was determined. Twenty micrograms of total cell lysate was resolved by SDS/PAGE using a Criterion TGX 4 to 20% precast gel (Bio-Rad) under reducing conditions and transferred to nitrocellulose membranes. The membranes were probed with a polyclonal α-mouse SLC30A8 rabbit Ab (custom-made from Thermo Fisher Scientific) and detected using an enhanced chemiluminescence detection system. The SLC30A8 polyclonal Ab was raised against a peptide spanning amino acids 29 to 43 of mouse SLC30A8 protein.

R138X Overexpression and Proteasomal Inhibition. Human *Slc30a8* WT and the first 137 amino acids followed by a stop codon were cloned with a C-terminal myc tag. HEK293 cells (0.4×10^6 cells per well) were seeded into a six-well plate. The next day, cells were transfected with 0.1 μg DNA per well using a Mirus TransIT-LT1, following the manufacturer's instructions. Two days after transfection, either DMSO or the proteasomal (10 μM MG-132 or 1 μM epoxomicin) or lysosomal (10 μg/mL chloroquine salt) inhibitor was spiked in. Cells were harvested after a 6-h treatment in RIPA buffer. Cell lysate (30 μg) was analyzed by Western blotting.

RNA Extraction and qPCR Analysis. For RNA extraction for qPCR analysis, islets from four mice per genotype were pooled and resuspended in 1 mL QIAzol reagent (79306; Qiagen). Samples were homogenized on a custom homogenizer (SKU 51-000-1; Omni) at 20,000 rpm for 180 s. Lysates were phase-separated with chloroform, and the aqueous phase was purified on the KingFisher Flex (5400630; Thermo Fisher Scientific) with the MagMAX-96 for Microarrays Total RNA Isolation Kit (AM1839; Thermo Fisher Scientific) with an additional DNase (79254; Qiagen) step added between the first and second washes. RNA was quantified on the NanoDrop (ND-8000-GL; Thermo Fisher Scientific) according to the manufacturer's protocol.

Between 37.5 and 375 ng of RNA, per RT-qPCR assay to be run, was mixed with SuperScript VILO Master Mix (11755500; Thermo Fisher Scientific) and cycled according to the manufacturer's instructions. The cDNA was diluted with nuclease-free water to between 0.5 and 5 ng/μL. RT-qPCR assays were done by combining water, master mix (4370074, Thermo Fisher Scientific or CSA-01113, Bioline), and 20× assay mix. The assay mix is a commercially available mixture of forward and reverse primers combined with a fluorescently labeled and quenched probe sequence (351372, Thermo Fisher Scientific or DLO-RFBL-MIX, LGC Biosearch). Samples were run in triplicate on a 384-well plate (4343370; Thermo Fisher Scientific) by pipetting 5 μL diluted cDNA and 10 μL of the appropriate RT-PCR assay mixture into each well. The 384-well plate was covered with an optically clear seal (16985-001; Agilent), spun down, and read on an ABI 7900HT Fast Real-Time PCR System with the 384-Well Block Module and Automation Accessory (4329002; Thermo Fisher Scientific) for 40 cycles according to the specifics of the master mix used. The sequences of the probe and primers are as follows: probe: 5′-TCCAAAACTGGGCAGTGAGTTCAACA-3′; forward primer: 5′-AATTGCAGTGCTGCTTTGC-3′; reverse primer: 5′-AGCTGC-GGCTGTTGTTGTC-3′.

RNA Sequencing Sample Preparation. Islets were isolated as described above and incubated overnight at 37 °C. The next day, 500 islets per genotype were picked into TRIzol (Invitrogen) as one sample and kept at −80 °C until RNA extraction and sequencing. Five different WT samples and four different R138X samples were analyzed. Total RNA was purified from all samples using the MagMAX-96 for Microarrays Total RNA Isolation Kit (Ambion by Life Technologies) according to the manufacturer's specifications. Genomic DNA was removed using MagMAX TURBO DNase buffer and TURBO DNase from the MagMAX kit listed above (Ambion by Life Technologies). mRNA was purified from total RNA using the Dynabeads mRNA Purification Kit (Invitrogen). Strand-specific RNA-seq libraries were prepared using the KAPA mRNA-Seq Library Preparation Kit (Kapa Biosystems). Twelve-cycle PCR was performed to amplify libraries. Sequencing was performed on a HiSeq 2500 (Illumina) by a multiplexed single-read run with 33 cycles.

RNA-Seq Read Mapping and Statistical Analysis of Differentially Expressed RNA. Raw sequence data (BCL files) were converted to FASTQ format via Illumina bcl2fastq v2.17. Reads were decoded based on their barcodes, and read quality was evaluated with FastQC (www.bioinformatics.babraham.ac.uk/projects/fastqc/). Reads were mapped to the mouse genome (National Center for Biotechnology Information GRCm38) using Array Studio software (OmicSoft) allowing two mismatches. Reads mapped to the exons of a gene were summed at the gene level. Differentially expressed genes were identified by the DESeq2 package (24), and significantly perturbed genes were

defined with fold changes of no less than 1.5 in either the up or down direction and with *P* values of at least 0.01.

Data Analyses. Data are reported as mean ± SEM. Statistical analyses were performed using Prism 6.0 (GraphPad Software). All parameters were analyzed by two-way ANOVA (**P*) or Student's *t* test (no significance was found). $*P < 0.5$, $**P < 0.01$, $***P < 0.001$, $****P < 0.0001$.

ACKNOWLEDGMENTS. We thank Angelos Papatheodorou for serum chemistry analysis, Lawrence Miloscio for help with islet isolation, the Regeneron DNAcore for RNA isolation and qPCR and Next Generation Sequencing analysis, Jinrang Kim for helpful discussions, and Haruka Okamoto for help with the manuscript. G.A.R. was supported by a Wellcome Trust Senior Investigator Award (WT098424AIA), the MRC Programme [MR/J0003042/1; MR/N00275X/1; MR/L020149/1 (DIVA)], Royal Society Wolfson Research Merit Awards, and Diabetes UK Project Grants (BDA11/0004210; BDA/15/0005275).

1. Dodson G, Steiner D (1998) The role of assembly in insulin's biosynthesis. *Curr Opin Struct Biol* 8:189–194.
2. Lemaire K, et al. (2009) Insulin crystallization depends on zinc transporter ZnT8 expression, but is not required for normal glucose homeostasis in mice. *Proc Natl Acad Sci USA* 106:14872–14877.
3. Nicolson TJ, et al. (2009) Insulin storage and glucose homeostasis in mice null for the granule zinc transporter ZnT8 and studies of the type 2 diabetes-associated variants. *Diabetes* 58:2070–2083.
4. Rutter GA, et al. (2016) Intracellular zinc in insulin secretion and action: A determinant of diabetes risk? *Proc Nutr Soc* 75:61–72.
5. Flannick J, et al.; Go-T2D Consortium; T2D-GENES Consortium (2014) Loss-of-function mutations in SLC30A8 protect against type 2 diabetes. *Nat Genet* 46:357–363.
6. Holbrook JA, Neu-Yilik G, Hentze MW, Kulozik AE (2004) Nonsense-mediated decay approaches the clinic. *Nat Genet* 36:801–808.
7. Tamaki M, et al. (2013) The diabetes-susceptible gene SLC30A8/ZnT8 regulates hepatic insulin clearance. *J Clin Invest* 123:4513–4524.
8. Schäffer L, et al. (2008) A novel high-affinity peptide antagonist to the insulin receptor. *Biochem Biophys Res Commun* 376:380–383.
9. Matsuoka TA, et al. (2004) The MafA transcription factor appears to be responsible for tissue-specific expression of insulin. *Proc Natl Acad Sci USA* 101:2930–2933.
10. Zhao Q, et al. (2015) The voltage-gated proton channel Hv1 is expressed in pancreatic islet β-cells and regulates insulin secretion. *Biochem Biophys Res Commun* 468:746–751.
11. Wang X, et al. (2017) The voltage-gated proton channel Hv1 is required for insulin secretion in pancreatic β cells. bioRxiv:10.1101/097816.
12. Qiu F, et al. (2016) Molecular mechanism of Zn^{2+} inhibition of a voltage-gated proton channel. *Proc Natl Acad Sci USA* 113:E5962–E5971.
13. Pound LD, et al. (2009) Deletion of the mouse Slc30a8 gene encoding zinc transporter-8 results in impaired insulin secretion. *Biochem J* 421:371–376.
14. Pound LD, et al. (2012) The physiological effects of deleting the mouse SLC30A8 gene encoding zinc transporter-8 are influenced by gender and genetic background. *PLoS One* 7:e40972.
15. Wijesekara N, et al. (2010) Beta cell-specific Znt8 deletion in mice causes marked defects in insulin processing, crystallisation and secretion. *Diabetologia* 53:1656–1668.
16. Hardy AB, et al. (2012) Effects of high-fat diet feeding on Znt8-null mice: Differences between β-cell and global knockout of Znt8. *Am J Physiol Endocrinol Metab* 302:E1084–E1096.
17. Mitchell RK, et al. (2016) Molecular genetic regulation of Slc30a8/ZnT8 reveals a positive association with glucose tolerance. *Mol Endocrinol* 30:77–91.
18. Wiederkehr A, Wollheim CB (2012) Mitochondrial signals drive insulin secretion in the pancreatic β-cell. *Mol Cell Endocrinol* 353:128–137.
19. De Marchi U, et al. (2017) A novel ATP-synthase-independent mechanism coupling mitochondrial activation to exocytosis in insulin-secreting cells. *J Cell Sci* 130:1929–1939.
20. Henquin JC (2000) Triggering and amplifying pathways of regulation of insulin secretion by glucose. *Diabetes* 49:1751–1760.
21. Ivarsson R, et al. (2005) Redox control of exocytosis: Regulatory role of NADPH, thioredoxin, and glutaredoxin. *Diabetes* 54:2132–2142.
22. Swisa A, et al. (2015) Loss of liver kinase B1 (LKB1) in beta cells enhances glucose-stimulated insulin secretion despite profound mitochondrial defects. *J Biol Chem* 290:20934–20946.
23. Valenzuela DM, et al. (2003) High-throughput engineering of the mouse genome coupled with high-resolution expression analysis. *Nat Biotechnol* 21:652–659.
24. Love MI, Huber W, Anders S (2014) Moderated estimation of fold change and dispersion for RNA-seq data with DESeq2. *Genome Biol* 15:550.